REVISTA INVESTIGACIÓN OPERACIONAL VOL. 44, NO. 2, 184-205, 2023

EXPLORATORY STUDY ON ESTIMATION, DETECTION AND ROBUSTNESS OF A DISCRETE SHAPELET TRANSFORM II

Damian Valdés-Santiago*†, Ángela León-Mecías*, Marta L. Baguer Díaz-Romañach*,
Manuel González-Hidalgo**,****,*****, and Antoni Jaume-i-Capó***,****
[1]Faculty of Mathematics and Computer Science, University of Havana, Cuba.
[2]SCOPIA Research Group, Department of Mathematics and Computer Science,
University of Balearic Islands, Spain.
[3]Computer Graphics and Vision and AI Group (UGiVIA), Research Institute of Health
Sciences, Mathematics and Computer
Science Department, University of Balearic Islands, Spain.
[4]Laboratory of Artificial Intelligence Applications (LAIA@UIB), University of
Balearic Islands, Palma, Spain.
[5]Balearic Islands Health Research Institute (IdISBa), Spain.

ABSTRACT

The Discrete Shapelet Transform II is designed to detect patterns, locating them in time and frequency. This transform solves a system of nonlinear equations to obtain the high–pass filter of the pattern–adapted wavelet (shapelet). This paper presents an exploratory study case to inquire about the impact of the numerical method for estimating shapelets, considering numerical indicators and the detection of two artificial patterns. Powell's method with Anderson pre–iteration get orthogonal, perfect reconstruction, finite impulse response, near–linear phase and compact support filters. For pattern detection, we take the detail coefficient with the highest value of the normalized measure $\mathbb{S}$, instead of $\mathbb{S} = 1$ used in the original publications. Compared to other wavelet filters, higher values of $\mathbb{S}$ were obtained where the pattern was inserted. Accurate detection of repeated patterns and robust detection when modifying the amplitudes were obtained. Modest noise robustness of detection was verified. The results showed the need for further study to evaluate the impact of the numerical method and the choice of the initial guess to estimate the shapelet using a larger number of numerical methods, patterns and signals. As a consequence of the analysis and discussion, we suggest new research questions about this transform to be answer in further research.

KEYWORDS: Wavelet filter design, Adapted wavelet, Time-frequency-shape joint analysis, Discrete Shapelet Transform, Discrete Wavelet Transform.

MSC: 65T60, 42C40, 65F99, 65H10

†Correspondence author: dvs89cs@matcom.uh.cu, dvs89cs@gmail.com/

RESUMEN
La Transformada *Shapelet* Discreta II está diseñada para detectar patrones, localizándolos en tiempo y frecuencia. En dicha transformada se resuelve un sistema de ecuaciones no lineales para obtener el filtro de paso alto de la wavelet adaptada a un patrón (*shapelet*). Esta investigación presenta un estudio exploratorio de casos cuyo objetivo fue indagar sobre el impacto del método numérico para estimar *shapelets*, considerando indicadores numéricos y la detección de dos patrones artificiales. El método de Powell con pre–iteración de Anderson permitió estimar filtros ortogonales, de reconstrucción perfecta, con respuesta finita al impulso, fase casi lineal y soporte compacto. Para detectar el patrón se tomó el coeficiente de detalle con mayor valor de la medida normalizada $\mathbb{S}$, en lugar de $\mathbb{S} = 1$ usado en las publicaciones originales. Respecto a otros filtros wavelet, se obtuvieron valores mayores de $\mathbb{S}$ donde se insertó el patrón. Se logró la detección precisa de patrones repetidos y una detección robusta al modificar su amplitud. Se verificó la modesta robustez de la detección ante el ruido. Los resultados mostraron la necesidad de un estudio más profundo para evaluar el impacto del método numérico y la elección de la aproximación inicial para estimar la shapelet, utilizando un número mayor de métodos, patrones y señales. Como consecuencia del análisis y discusión, se sugieren preguntas de investigación a responder próximamente.

PALABRAS CLAVE: Diseño de filtros wavelet, Wavelet adaptada, Análisis conjunto tiempo-frecuencia-forma, Transformada Shapelet Discreta, Transformada Wavelet Discreta.

1. INTRODUCTION

In the last two decades, among the numerous fields where wavelets have been widely applied, there are different techniques to create wavelet transforms that match a specified signal, see for instance [11]. The idea of adapting a wavelet to specific problems, i.e., to create and use data-dependent wavelets, has been developed for various purposes, for example, biological pattern recognition [3], iris recognition system [14], and detection of the QRS of an electrocardiogram signal [8], among others.
We are interested in the proposal made by Guido and colleagues [5, 6, 7]. They constructed adapted wavelets with the Discrete Shapelet Transform (DST), which determines the time support of the frequencies and a pattern shape. The DST-I [7] include a constraint based on fractal dimension, and solve the nonlinear equations system (NLS) formed by this constraint and others of unit energy, vanishing moments and orthogonality. Its computational cost is high. Therefore, DST-II [5] replaced the fractality constraint with two pattern correlation constraints. In the third version, DST-III [6], it was proposed to obtain nearly symmetric wavelets by changing the vanishing moments constraint by a symmetry constraint [10].
According to the original publications, this NLS can be solved "by any iterative numerical procedure" (see [5, p. 10 and p. 11] and [6, p. 3]) to obtain the coefficients of the high-pass filter of the shapelet. The cited studies show two numerical examples of shapelets for artificial patterns and experiments on detecting seven patterns from the visual system of a fly. In these experiments, it is not specified which numerical algorithm was used to find the NLS solution, nor which was the initial guess used for iteration; a key aspect in the convergence [16].
When we decided to use the DST-II algorithm, we didn't find in [5, 6, 7] which numerical algorithm was used for solving the NLS, so we realized that this is a very relevant aspect. Therefore, this paper presents an exploratory study case whose objective is to inquire about the impact of the numerical

method to estimate shapelets, considering numerical indicators and the detection of two patterns gave in the original publications [5, 6]. The pattern detection robustness to repetitions, amplitude variations, contractions of these patterns, as well as robustness to noise, are also examined. The pattern detection is compared with other wavelet filters.
The results showed the need for further study to evaluate the impact of the numerical method and the choice of the initial guess to estimate the shapelet using a larger number of numerical methods, patterns and signals.
The paper is structured as follows: Section 2. introduces basic concepts and elements of DST-II, as well as the NLS under study. Section 3. is devoted to the theoretical aspects of system's solution algorithms used in the experiments. This is followed by the design of the experiments (section 4.), and the results for both study cases, as well as their discussion (section 5.). Finally, we suggest new research questions to be answered in future studies.

2. DISCRETE SHAPELET TRANSFORM II

The DST-II [5] proposes a way of constructing wavelets, which not only finds the temporal support of the frequencies appearing in a given signal, but also the shape, hence its name shapelet. In analogy to the construction of wavelet bases, high-pass filters and low-pass filters that define the scaling and wavelet functions are needed.
This transform has the following constraints for the high–pass filter coefficients q: i) the filter support size is $N \geq 6$ and necessarily even to have perfect reconstruction [17]; and ii) the pattern $m[\cdot]$ must have odd size equal to $N + 1$.
The NLS $\mathbf{F}(q_0, q_1, \cdots, q_{N-1}) = \mathbf{0}$ of N equations and N unknowns is as follows:

- Unitary energy:
$$\left(\sum_{k=0}^{N-1} q_k^2 \right) - 1 = 0; \tag{2.1}$$
- $\frac{N}{2} - 2$ vanishing moments for the wavelet:
$$\sum_{k=0}^{N-1} q_k \cdot k^b = 0, \tag{2.2}$$
where $b = 0, 1, \cdots, \frac{N}{2} - 3$;
- $\frac{N}{2} - 1$ orthogonality conditions:
$$\sum_{k=0}^{N-2l-1} q_k \cdot q_{k+2l} = \delta_{0,l}, \tag{2.3}$$
where δ is the Dirac's delta function and $l \in [1, N/2 - 1]$; and
- two matching conditions for detecting the pattern:
$$\sum_{k=0}^{N-1} q_k \cdot m_k = 0, \quad \sum_{k=0}^{N-1} q_k \cdot m_{k+1} = 0. \tag{2.4}$$

To obtain the perfect reconstruction filter bank [17] of a DST-II the following filters are computed:

- $p[\cdot]$ and $q[\cdot]$, where $p_k = (-1)^k \cdot q_{N-k-1}$ $(0 \leq k \leq N-1)$, forming finite impulse response (FIR) filters with an even support size, N; and
- $\overline{p}[\cdot]$ and $\overline{q}[\cdot]$, where $\overline{p}_k = p_{N-k-1}$ and $\overline{q}_k = (-1)^{k+1} \cdot p_k$, characterizing the synthesis filter bank.

The DST-II will be used to decompose a signal, modify its coefficients and reconstruct it. The more modifications are made to the coefficients, the more the reconstructed signal will resemble the shape of the DST-II scale and wavelet functions [3]. That is why, the major shapelet function, $\Gamma(x) = \sum_k p_k \cdot \Gamma(2N-k)$, and the minor shapelet function, $\Theta(x) = \sum_k q_k \cdot \Gamma(2N-k)$ are computed, similar to the scale and wavelet functions of the Discrete Wavelet Transform [17].

3. NUMERICAL METHODS FOR FINDING THE FILTER OF A DST-II

To obtain the coefficients of the shapelet high-pass filter q, the NLS described above, must be solved. There are several methods to solve it, but the convergence depends on the initial guess of the iteration and certain theoretical characteristics of the methods. In what follows, we present a brief overview of three methods we used. These methods start from a predefined initial guess, typically, the null vector [15, 16].

3.1. Powell's method

Powell's method [15] is based on Newton's algorithm. At each iteration of the Newton's algorithm, if the solution lies within the confidence region, then Powell's method is used to update the solution, otherwise it is used to find the minimum of the objective function in the direction of gradient descent. If the minimum point known as the Cauchy point is outside the confidence region, then it is truncated to the boundary of the confidence region and taken as the new solution. If the Cauchy point is inside the confidence region, the new solution is taken at the intersection between the boundary of the confidence region and the line joining the Cauchy point and the Newton method solution [15]. This method is implemented in MINPACK-1 [12] as `HYBRD`. Its number of operations is $\mathcal{O}(N^2)$ per function call and requires $(3N^2 + 17N)/2$ for storage memory.

3.2. Broyden's method with scalar approximation of the Jacobian

Broyden's methods [15] are based on a quasi–Newton algorithm. They differ in the way they use to replace the Jacobian matrix [16]. These methods have superlinear convergence, require N function evaluations per iteration, and $\mathcal{O}(N^2)$ operations. When the iteration matrix is constructed with a scalar approximation of the Jacobian, this method is called linear mixing.

3.3. Anderson's method

Let the input and output vectors, respectively, of the M iterations to be considered be: $\overline{x}^{(k)} := x^{(k)} + \sum_{j=1}^{M} \vartheta_j^{(k)} \left(x^{(k-j)} - x^{(k)} \right)$, where $0 \leq M \leq k-1$. The coefficients $\vartheta_j^{(k)}$ are sought such that the

linear combination minimizes the norm of the general residual vector. For this purpose, a system of linear equations whose solution are the coefficients $\vartheta_j^{(k)}$ is solved [1]. Once the optimal linear combination has been found, the input vector is set for the following iteration: $x^{(k+1)} = \overline{x}^{(k)} + \beta^{(k)}\overline{R}^{(k)}$, where $\beta^{(k)}$ is the mixing parameter and $\overline{R}^{(k)}$ the residual. Anderson's method needs the storage for the $(2M+2)N-$component vectors $x^{(k)}$ and $R^{(k)}$, of the current and previous M iterations, and, in addition, the solution of a linear system of order M.

4. EXPERIMENTAL DESIGN

a) Two study cases were considered corresponding to two artificial patterns taken from the original publications [5] and [6], respectively:

- Pattern $m_1[\cdot]$ with support size $N + 1 = 8 + 1 = 9$ and coordinates (*sample number, amplitude*): (0, 0.20); (1, 0.50); (2, 0.45); (3, 0.85); (4, 0.80); (5, -0.75); (6, 0.25); (7, 0.20) and (8, 0.55).
- Pattern $m_2[\cdot]$ of size $N + 1 = 12 + 1 = 13$ and coordinates: (0, 0.01); (1, 0.01); (2, 0.01); (3, 0.02); (4, 0.05); (5, 0.23); (6, 0.62); (7, 0.90); (8, 0.98); (9, 0.88); (10, 0.02); (11, 0.01) and (12, 0.01).

b) Construction of the DST-II filter bank: The NLS to obtain q was symbolically encoded in `SymPy` and solved independently for the two artificial patterns considered with Powell's hybrid method (`hybr`) from three initial guesses: the null vector (`null`), the solution from `linear mixing` method, and the one from Anderson's method (`anderson`). The MINPACK-1 [12, 15] routines implemented in the Python package `scipy.optimize.root` [18] were used.

c) Seven experiments were performed with double numerical precision:

- *Experiment I*: Using the numerical methods describe above, and considering the two artificial patterns that appear in [5, 6], the resulting shapelet functions were compared with those obtained in the cited works. We also examine the effect of the choice of initial guess on methods' convergence. From the numerical point of view, for each NLS solution we reported the number of $\mathbf{F}$ evaluations (Evals.), the norm of the residual ($||\mathbf{F}(q^*)||_2$), and the distance $||q_{\text{Guido (2018/2021)}} - q^*||_2$ to the filters from original publications [5, 6]. In addition, the corresponding minor and major shapelets were obtained using the cascade algorithm [17] with 8 levels, implemented in `PyWavelets` [9]. To evaluate the quality of the filters from a signal processing point of view, their frequency and phase response are computed and plotted, in addition to the corresponding zeros plot [13].
- *Experiment II*: Evaluation of shapelet performance in pattern detection. To achieve this, we inserted the patterns ($m_1[\cdot]$ and $m_2[\cdot]$) at position 41 in two signals ($f_1[\cdot]$ and $f_2[\cdot]$)

with 64 samples, given in [5, 6]:

$$f_1[\cdot] = \begin{cases} \cos\left(\frac{27}{8}\cdot\pi\cdot i\right)\cdot\sin\left(\frac{75}{8}\cdot\pi\cdot i\right), & 0\leq i\leq 40, \\ m_1[i], & 41\leq i\leq 49, \text{ and} \\ \cos\left(\frac{295}{32}\cdot\pi\cdot i\right)\cdot\sin\left(\frac{105}{32}\cdot\pi\cdot i\right), & 50\leq i\leq 63 \end{cases} \tag{4.1}$$

$$f_2[\cdot] = \begin{cases} \cos\left(3,5\cdot\pi\cdot i\right)\cdot\sin\left(31,250\cdot\pi\cdot i\right), & 0\leq i\leq 40, \\ m_2[i], & 41\leq i\leq 53, \\ \cos\left(13,281\cdot\pi\cdot i\right)\cdot\sin\left(3,906\cdot\pi\cdot i\right), & 54\leq i\leq 63. \end{cases} \tag{4.2}$$

To perform the shapelet transform, the filter bank was constructed in PyWavelets. The detection was based on the normalized similarity measure $\mathbb{S} = e^{-(|\text{DST-II}(f[\cdot])|)^{\alpha}}$ $(0 < \alpha \leq 1)$, which emphasizes the presence of zeros in the DST-II($f[\cdot]$), with $f[\cdot]$ being the analyzed signal. In [5], the pattern was detected at the position where $\mathbb{S} = 1$. In our experiments this value was not reached. After a mathematical analysis of measure $\mathbb{S}$, we take as a criterion for pattern detection the index k of the shapelet coefficient with the highest value of $\mathbb{S}(\alpha = 0.1)$. Thus, the pattern $m[\cdot]$ is estimated to start at $f_{(k\cdot 2^j-1)}$ or $f_{(k\cdot 2^j)}$.

For next experiments, we choose the shapelet obtained with the most adequate initial guess, and perform the following experiments.

- *Experiment III*: To compare the detection of the selected shapelet with other wavelet filters, such as Haar, Daubechies with support sizes 4, 6, 8, 8, 10, 20, 30 and 38, and Symlet with support sizes 8 and 16, Coiflets with support sizes 6, 12 and 16. These filter sizes are similar to those used for comparison in [5, 6]. The prediction errors of the pattern occurrence in the signal were computed for each wavelet filter used.

- *Experiment IV*: To evaluate the detection of a repeated pattern in a signal.

- *Experiment V*: To evaluate stability in pattern detection when varying its amplitude.

- *Experiment VI*: To evaluate stability in pattern detection when shrinking (subsampling) the pattern by a factor of 2. Theoretically, DST-II should detect this subsampled version of the pattern at the second level of decomposition [4, 10].

In general, the algorithm to measure the similarity between the signal $f[\cdot]$ and the pattern of interest $m[\cdot]$ in a particular frequency subband j is:

i) Create the DST-II filter bank for the pattern $m[\cdot]$;

ii) Calculate the $j-$th DST-II level of $f[\cdot]$, with j being the subband of interest, $j \leq \frac{\log(N)}{\log(2)}, j \in \mathbb{Z}$;

iii) Take the index k of the shapelet coefficient with the largest value of $\mathbb{S}(\alpha = 0.1)$. Thus, the pattern $m[\cdot]$ is estimated to start at $f_{(k\cdot 2^j-1)}$ or $f_{(k\cdot 2^j)}$.

- *Experiment VII*: To evaluate the noise robustness adding Gaussian and Poisson noise to the signal using different noise levels. For each noise level, 30 noisy signals were obtained and the detection was performed. Thresholds for pattern detection errors were considered and the detection rate was computed for each noise level.

5. RESULTS AND DISCUSSION

This section presents the results of the seven experiments described above for two artificial patterns, and evaluating the detection robustness against a group of signal transformation. These patterns were used because the original papers publish the data to obtained it, also because they represent different behavior for a signal: the first pattern present one oscillation around zero and has wiggles; the second one is symmetric and positive, without oscillation around zero.

5.1. First study case: pattern $m_1[\cdot]$

Table 1 shows the numerical indicators of the NLS solutions for pattern $m_1[\cdot]$, using Powell's method from three initial guesses. Starting with `anderson` fewer systems evaluations are performed, and the most accurate solution was obtained. When compared with the solution reported in [5], the closest result was achieved starting from the `anderson` initial guess (0.56).

Initial guess/Pre–iteration	Evals.	$\|\|\mathbf{F}(q^*)\|\|_2$	$\|\|q_{\text{Guido (2018)}} - q^*\|\|_2$
`null`	56	$3{,}26147598401959 \cdot 10^{-12}$	1,27
`linear mixing`	113	$4{,}17346034158683 \cdot 10^{-12}$	1,51
`anderson`	11	$1{,}12228928558634 \cdot 10^{-13}$	0,56

Table 1: Numerical indicators of the NLS solution by shapelet construction for the pattern $m_1[\cdot]$.

Figure 1 plots filter properties such as frequency response, phase, and zeros plot, as well as the graphical representation of minor and major shapelets. Using `null` as the initial guess, a very irregular shapelet was obtained (Figure 1a), which is reflected in the nonlinear phase of the corresponding filters. Also, this shapelet had no frequency differentiation with respect to $\frac{\pi}{2}$ cutoff point. Smoother shapelets with nearly linear phase (Figure 1c) and better frequency differentiation were estimated for the rest of initial guesses.

For each filter obtained, the detection algorithm was applied to locate the pattern $m_1[\cdot]$ in the signal $f_1[\cdot]$. These detection results can be seen in Figure 2. It should be clarified that, given the detection constraints in the NLS, the shapelet can predict the pattern occurrence from its first or second position. In the calculation of prediction and error for this table, it was assumed that the shapelet locates the pattern at its first position.

Each subfigure in Figure 2 shows: the signal with the pattern highlighted in green (top), the DST-II (center) and the $\mathbb{S}$ measurement of the wavelet coefficients, where the coefficient selected by the detection algorithm (bottom) is marked (light blue dashed line). In yellow lines (top) the two positions where the pattern is located according to that algorithm are highlighted. The plots in the center and below show a purple dashed line separating the approximation and detail coefficients.

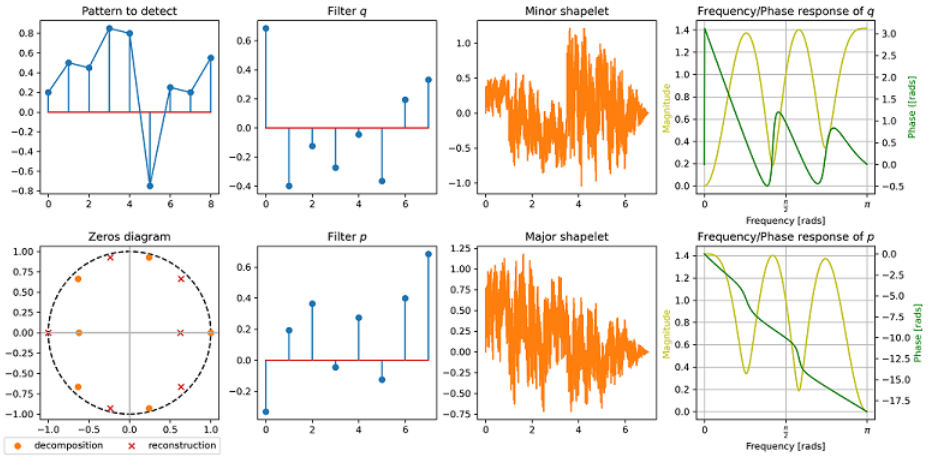

(a) Shapelet obtained from the initial guess `null`.

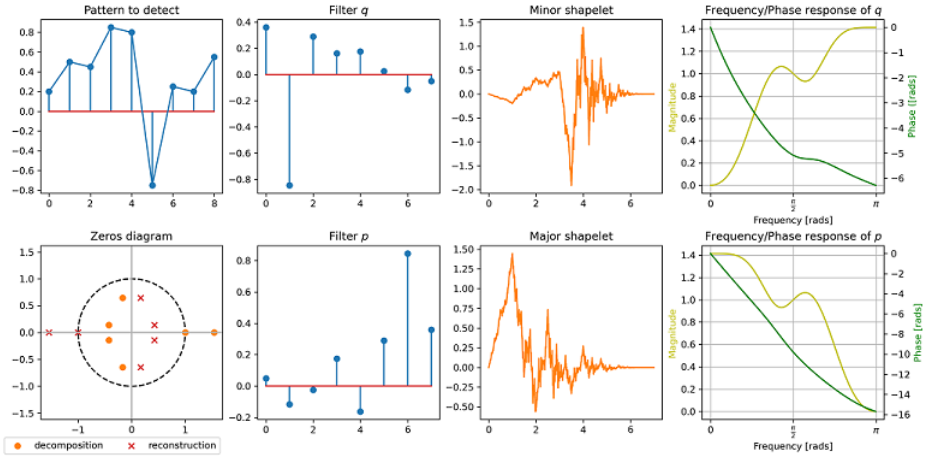

(b) Shapelet obtained from the initial guess `linear mixing`.

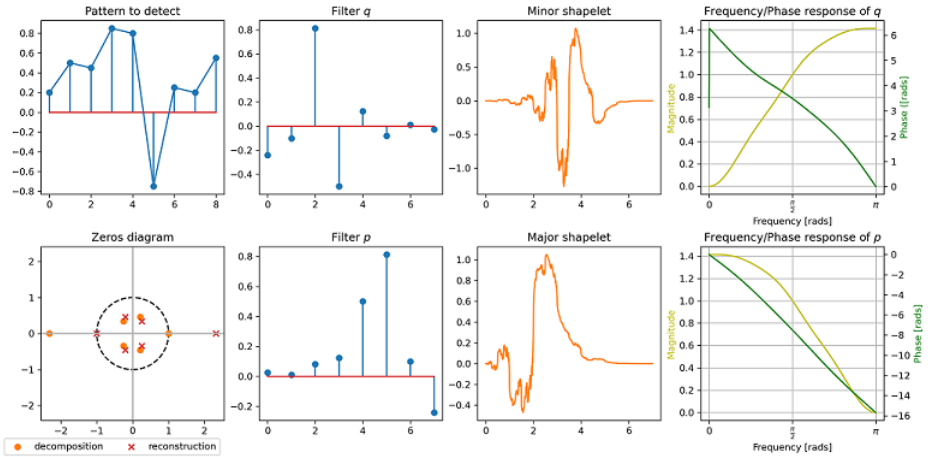

(c) Shapelet obtained from the initial guess `anderson`.

Figure 1: Filters q (high-pass) and p (low-pass) of the shapelet adapted for pattern $m_1[\cdot]$ with Powell's method, starting from three initial guesses.

It can be seen that all the initial guesses located the pattern with no error. Therefore, taking in account the good numerical indicators for `anderson` initial guess, from now on we will use the estimated shapelet with this starting point for the following experiments.

Using this shapelet, we compare the pattern detection against other wavelet filters. Figure 3 shows the values of $\mathbb{S}$ for the detail coefficients of signal $f_1[\cdot]$ decomposed using the shapelet and 13 other wavelet filters. Only the shapelet detect the pattern with high precision.

By tripling the signal $f_1[\cdot]$, three occurrences of the pattern were obtained at positions 41, 105 and 169. In Figure 4, the pattern is highlighted in green (top), the DST-II of the signal (center) and the measure $\mathbb{S}$ for detail shapelet coefficients (bottom) are shown. The coefficients selected by the detection algorithm are marked (light blue dashed line). Yellow lines (top) highlight the positions where the pattern is located according to the algorithm. The plots in the center and below show a purple dashed line separating the approximation and detail coefficients.

It can be seen that the generated filter bank for pattern $m_1[\cdot]$ was able to detect the three occurrences of the pattern, corresponding to the positions of the detail shapelet coefficients with the three highest values of the measure $\mathbb{S}$, at positions 22, 86 and 150, respectively (Figure 4, see stitched vertical line).

By modifying the amplitude of pattern $m_1[\cdot]$ by 0.5 and 4 within signal $f_1[\cdot]$, the detection algorithm is successful with a one-sample error (Figure 5). This verifies the theoretical argument about the DST-II allowing the pattern shape to be detected, even when it appears amplified [4].

To examine the ability of DST-II for multilevel detection of the pattern for which it was constructed, the pattern was subsampled by a factor of 2.

Figure 6 shows the signal with the dilated pattern and highlighted in green (top), the DST-II of the signal (center) and the measure $\mathbb{S}$ for detail shapelet coefficients (bottom), the separation of the 2-level wavelet coefficients of the DST-II is marked (purple dashed line). Green and yellow dashed lines show the positions of the coefficients selected by the detection algorithm at both levels. Above, a green (yellow) line marks the prediction of pattern occurrence at level 1 (level 2) of DST-II.

Note that the DST-II detects the pattern at the first level of decomposition (green line), and not at the second one (yellow line), as expected. This might be due to the similarity between some fragments of the signal and the compressed pattern, which cause false negatives in the detection.

Incorporating together the pattern $m_1[\cdot]$ and its dilated version into the signal $f_1[\cdot]$ resulted in detecting the original pattern at level 1 of the decomposition and its subsampled version at level 2 at the correct positions, with one-sample error (Figure 7).

In this figure, the signal with the dilated pattern (position 4) and the pattern (position 43) is highlighted in green (top), the DST-II of the signal (center) and the measure $\mathbb{S}$ of the detail shapelet coefficients (bottom), the separation of the 2-level detail shapelet coefficients of the DST-II is marked (purple dashed line). Green and yellow dashed lines show the positions of the coefficients selected by the detection algorithm at both levels. Above, a green (yellow) line marks the prediction of pattern occurrence at level 1 (level 2) of DST-II. This corresponds with the theoretical assumption of multilevel localization of the pattern.

Table 2 shows the results of pattern $m_1[\cdot]$ detection for different noise values (σ and λ parameters of a Gaussian and Poisson distributions, respectively) using a detection threshold of 2 samples.

For both types of noise it is observed that by slightly perturbing the signal, the pattern is correctly

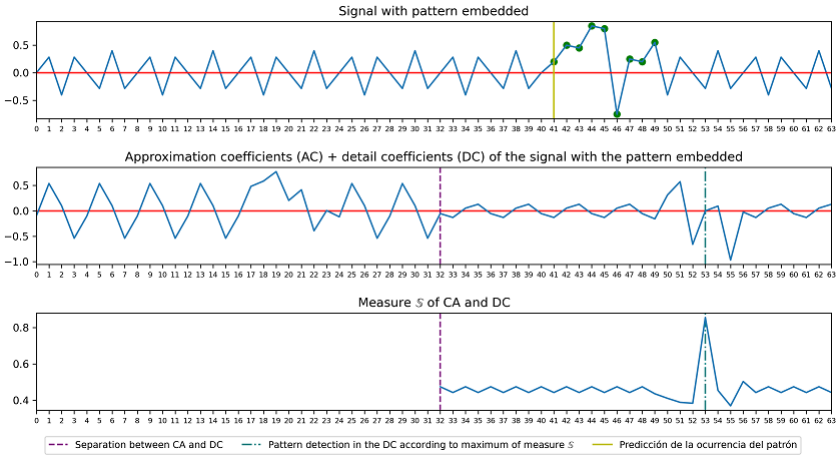

(a) Localization with the filter obtained from the initial guess `null`. Error = 0.

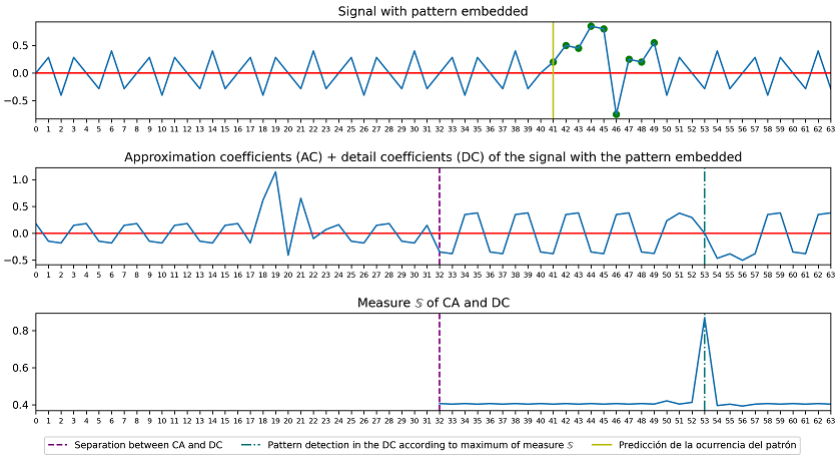

(b) Localization with the filter obtained from the initial guess `linear mixing`. Error = 0.

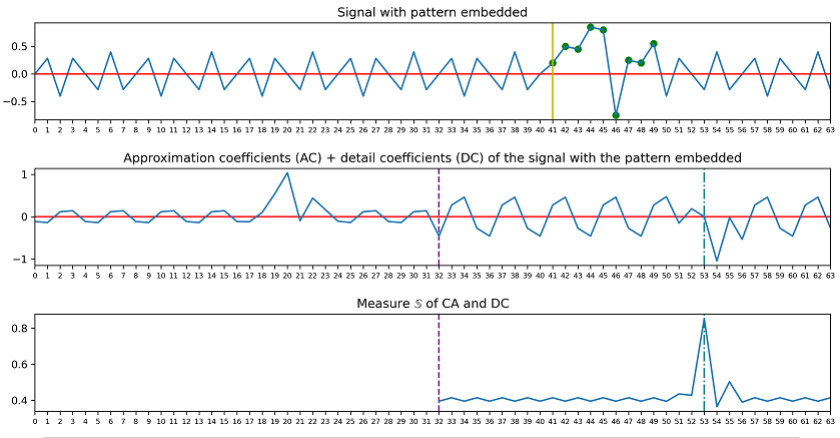

(c) Localization with the filter obtained from the initial guess `anderson`. Error = 0.

Figure 2: Localization of the pattern $m_1[\cdot]$ in the signal $f_1[\cdot]$ with the proposed detection algorithm.

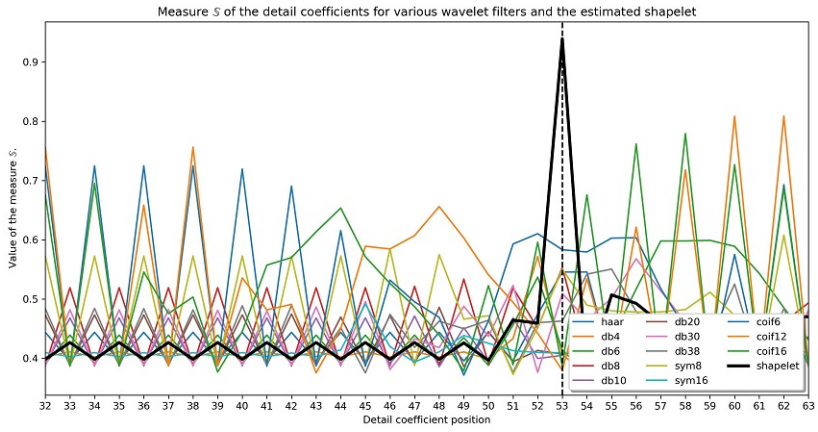

Figure 3: Similarity measure $\mathbb{S}$ for the shapelet (in black) and 13 other classical wavelet filters applied to signal $f_1[\cdot]$. Sample 53 is highlighted, which is the position where the pattern $m_1[\cdot]$ should be detected.

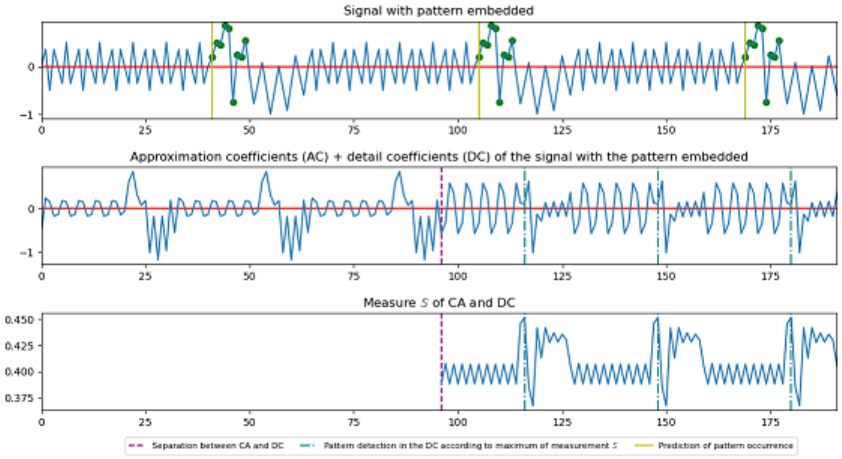

Figure 4: Detection of three repetitions of the pattern $m_1[\cdot]$ in a signal.

Gaussian noise			Poisson noise		
σ	Pattern detection counts	Detection rate	λ	Pattern detection counts	Detection rate
0.01	30	100%	0.01	24	80.00%
0.02	29	96.67%	0.02	16	53.33%
0.03	21	70.00%	0.03	19	63.33%
0.04	13	43.33%	0.04	13	43.33%
0.05	7	23.33%	0.05	8	26.67%

Table 2: Detection results for pattern $m_1[\cdot]$ after adding noise to the signal $f_1[\cdot]$. The pattern was detected with an error of up to 2 samples.

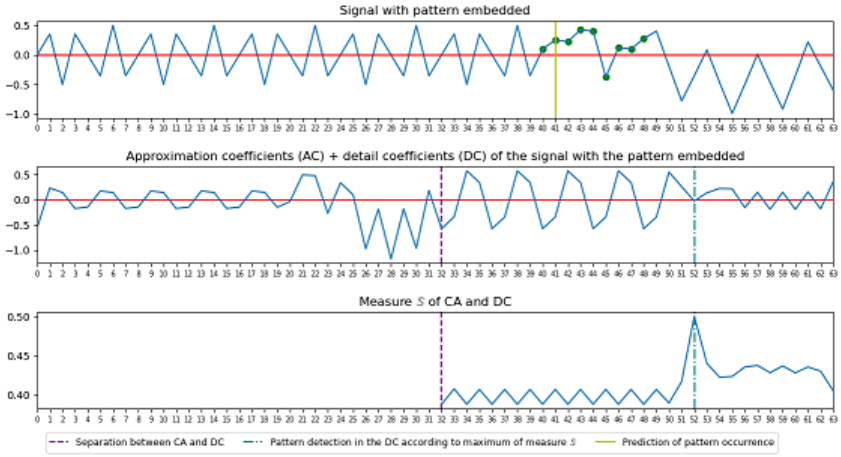

(a) Pattern amplitude modification by 0.5.

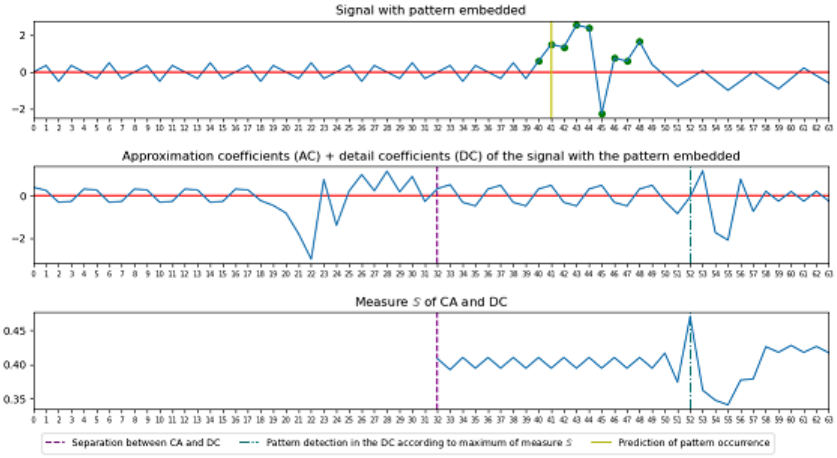

(b) Pattern amplitude modification by 3.

Figure 5: Detection of two amplified versions of pattern $m_1[\cdot]$ in the signal $f_1[\cdot]$.

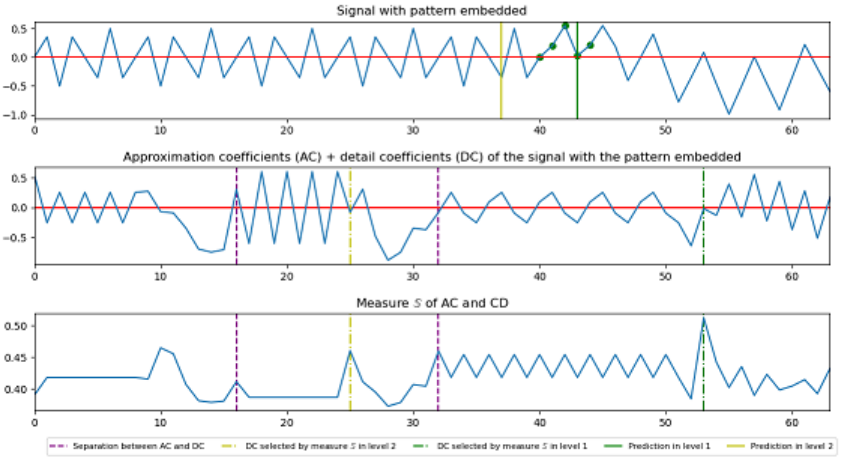

Figure 6: Detection of a dilated version of the pattern $m_1[\cdot]$.

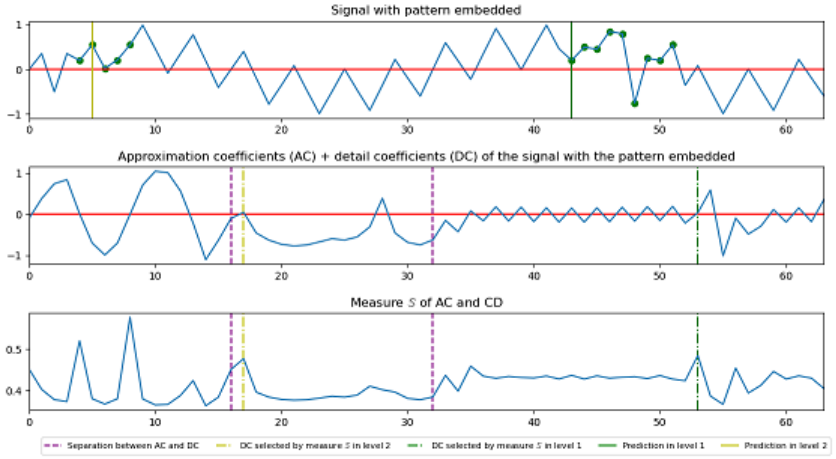

Figure 7: Joint detection of the pattern $m_1[\cdot]$ and its dilated version.

detected, but when increasing the noise level, the detection results become progressively worse, reflected in the decrease of the detection rate. This is consistent with the "modest robustness to noise" of DST-II mentioned in [5, 6].

5.2. Second study case: pattern $m_2[\cdot]$

Table 3 shows the numerical results referring to the solution of the system to adapt the shapelet to the pattern. For this purpose, three initial guesses were again taken. The Powell's method converged, except for the initial guess `linear mixing`. This algorithm performed fewer NLS evaluations when starting with `linear mixing` (35), but did not converge. The initial guess that obtained the most accurate solution was `anderson`. When compared with the solution reported in [6], the closest result was achieved starting from the aforementioned initial guess.

Initial guess/Pre–iteration	Evals.	$\|\|\mathbf{F}(q^*)\|\|_2$	$\|\|q_{\text{Guido (2021)}} - q^*\|\|_2$
`null`	57	1,63977362698396 $\cdot 10^{-10}$	1,49
`linear mixing`	35	1639398805595530	39252437,11
`anderson`	160	4,00892364240798 $\cdot 10^{-13}$	1,45

Table 3: Numerical indicators of the solution for the pattern $m_2[\cdot]$.

The estimated filters are shown in Figure 8, which exposes their frequency response properties, phase and zeros plot, as well as the plots of the minor and major shapelets. By using `linear mixing` as the initial guess, a very irregular shapelet was obtained, which is reflected in the nonlinear phase of the corresponding filter and the non-differentiation of frequencies. This is due to not convergence of the iteration, showed by a very large value of the residual. On the other hand, for `null` and `anderson` initial guesses, smoother shapelets were estimated with almost linear phase (Figure 8a and c) and better frequency differentiation.

The pattern detection results for each shapelet are shown in Figure 9. It can be noted that the initial guess `linear mixing` generates false negatives. By taking `null` and `anderson` guesses, the heuristic detected the pattern more accurately, as expected. Therefore, as in our fisrt study case, from now on we will use the estimated shapelet with `anderson` initial guess for the following experiments.

The values of $\mathbb{S}$ for the detail coefficients of signal $f_2[\cdot]$ decomposed using this shapelet and the other wavelet filters are shown in Figure 10. Only the shapelet detected it accurately.

By tripling the signal $f_2[\cdot]$, three occurrences of the pattern were obtained at positions 41, 105 and 169. In Figure 11 it can be seen that the constructed shapelet for $m_2[\cdot]$ was able to detect all occurrences of the pattern with a 2-samples error.

By modifying the amplitude of pattern $m_2[\cdot]$ by 0.5 and 3 within signal $f_2[\cdot]$, the pattern was successfully detected when modified by a factor of 3, and with a 4-samples error using a factor of 0.5 (Figure 12). This verifies the theoretical argument in [5].

To examine the ability of DST-II for multilevel detection, the pattern $m_2[\cdot]$ was subsampled by a factor of 2. The detection had a 1-sample error (Figure 13). By incorporating the subsampled pattern into the same signal, the original pattern was successfully detected in level 1 of the decomposition (Figure

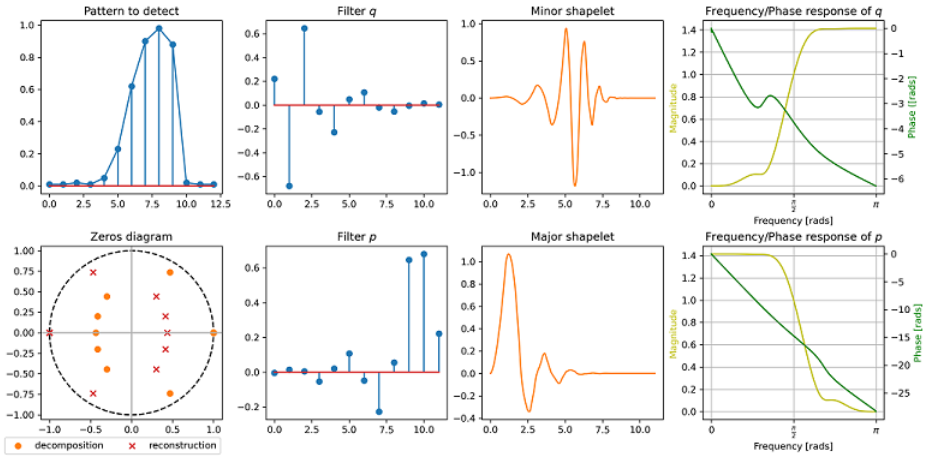

(a) Shapelet obtained from the initial guess `null`.

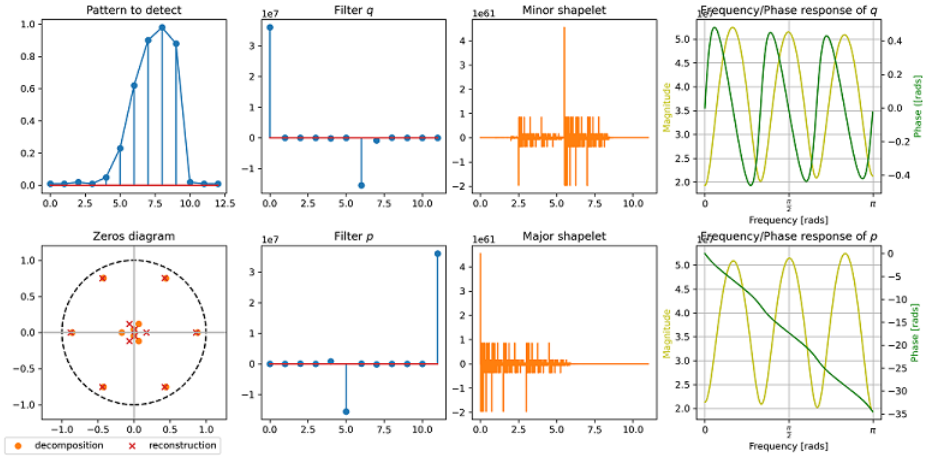

(b) Shapelet obtained from the initial guess `linear mixing`.

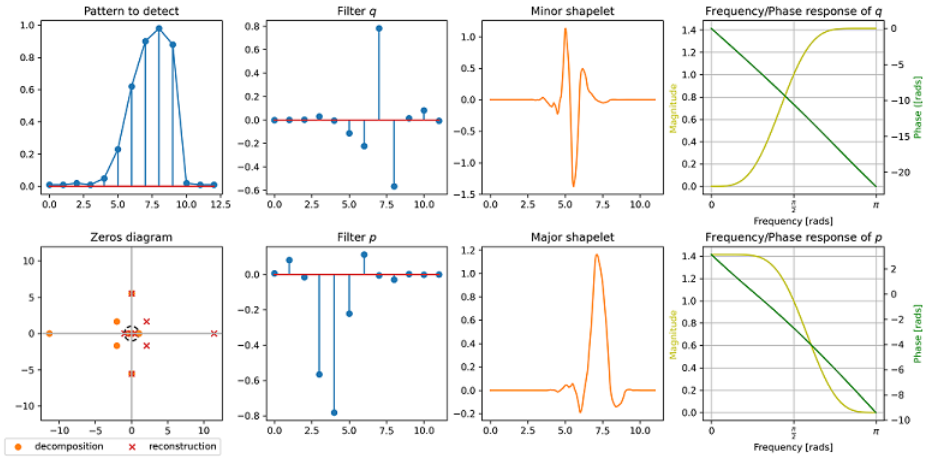

(c) Shapelet obtained from the initial guess `anderson`.

Figure 8: Filters q (high pass) and p (low pass) for the adapted pattern $m_2[\cdot]$ with Powell's method, starting from three initial guesses.

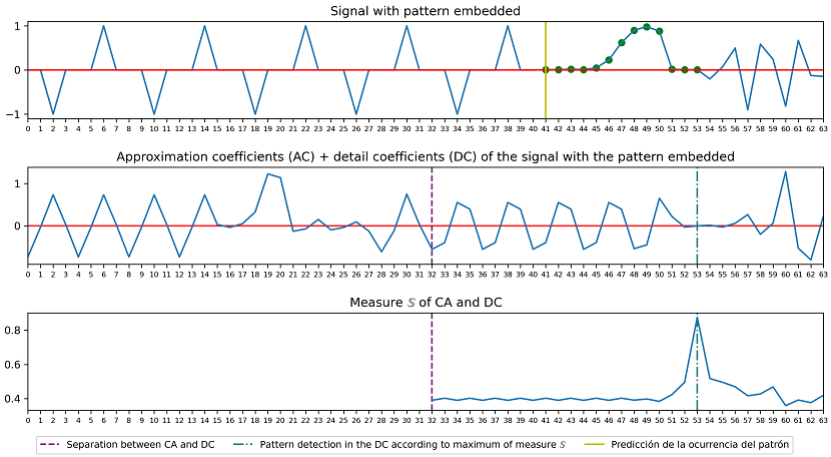

(a) Localization with the filter obtained from the initial guess `null`. Error = 0.

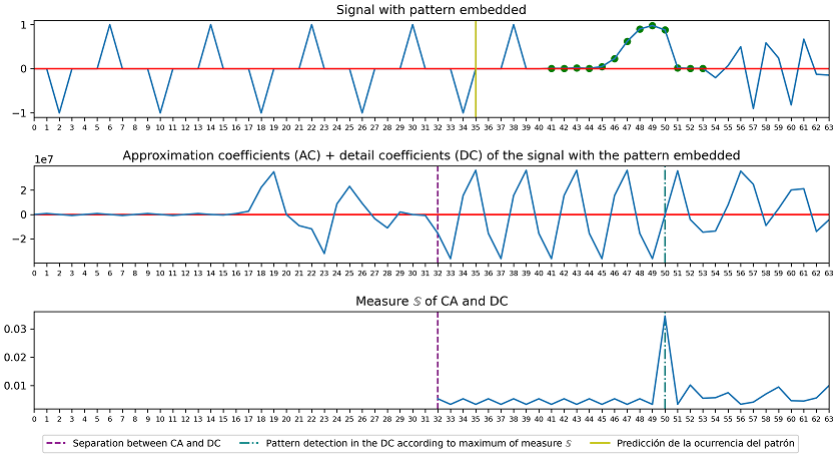

(b) Localization with the filter obtained from the initial guess `linear mixing`. Error = 5.

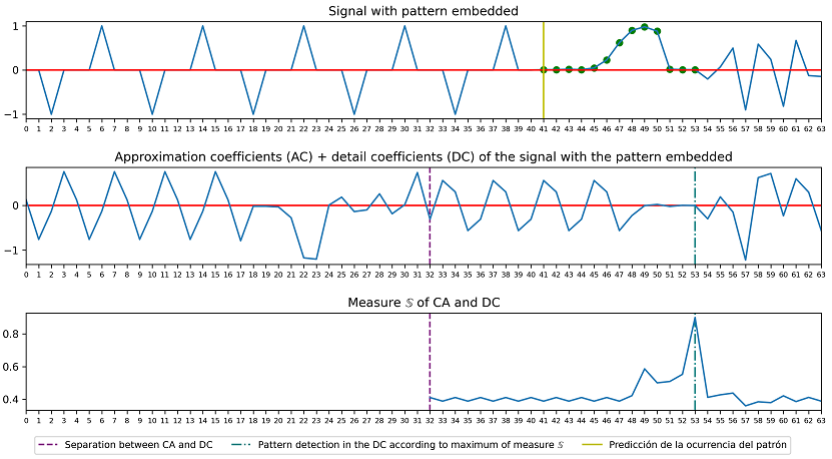

(c) Localization with the filter obtained from the initial guess `anderson`. Error = 0.

Figure 9: Localization of the pattern $m_2[\cdot]$ in the signal $f_2[\cdot]$ with the proposed detection algorithm.

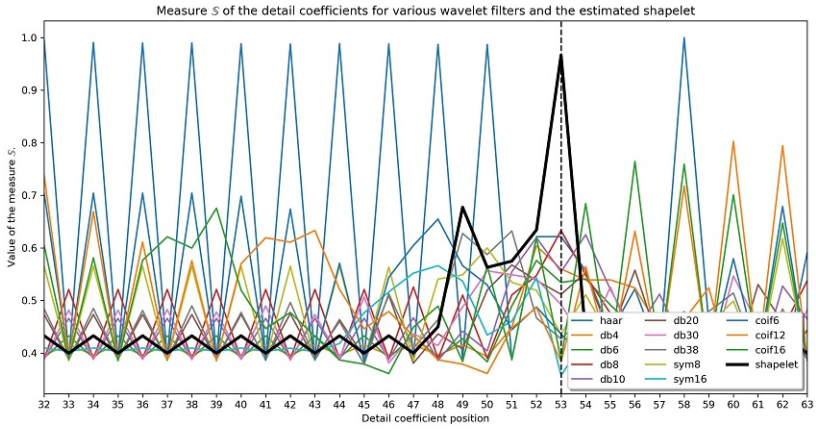

Figure 10: Similarity measure $\mathbb{S}$ for the shapelet (in black) and 13 other classical wavelet filters applied to signal $f_2[\cdot]$. Sample 53 is highlighted, which is the position where the pattern $m_2[\cdot]$ should be detected.

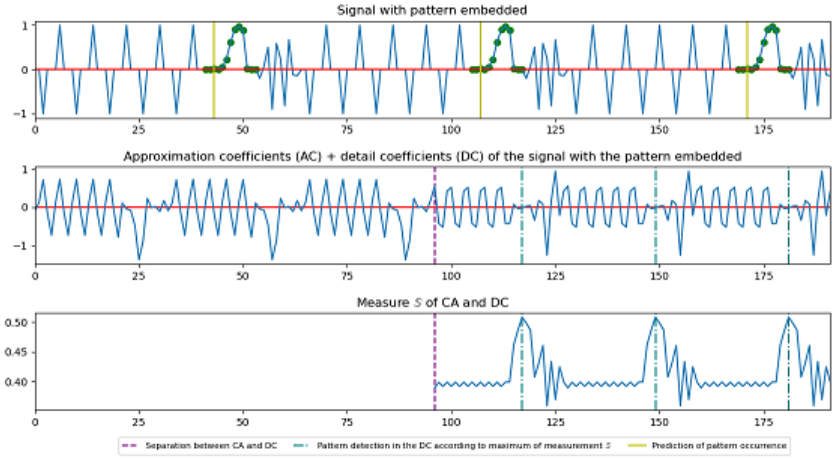

Figure 11: Detection of three repetitions of the pattern $m_2[\cdot]$ in a signal.

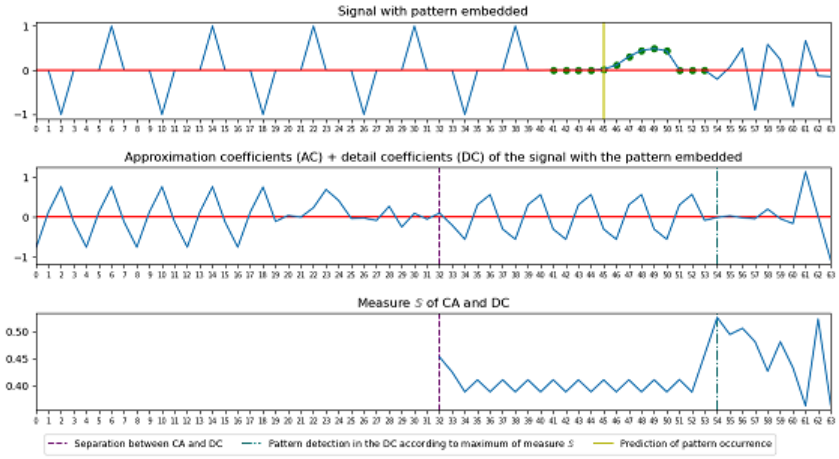

(a) Pattern amplitude modification by 0.5.

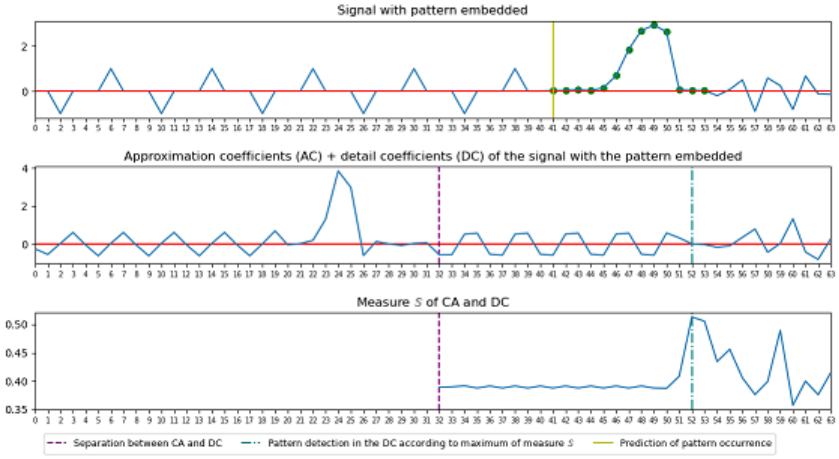

(b) Pattern amplitude modification by 3.

Figure 12: Detection of two amplified versions of pattern $m_2[\cdot]$ in the signal $f_2[\cdot]$.

14). However, the detection algorithm based on the measure $\mathbb{S}$ fails to detect the dilated version at level 2, although it is observed that at position 30 the second maximum of that measure is reached, which corresponds to the correct position of the subsampled pattern.

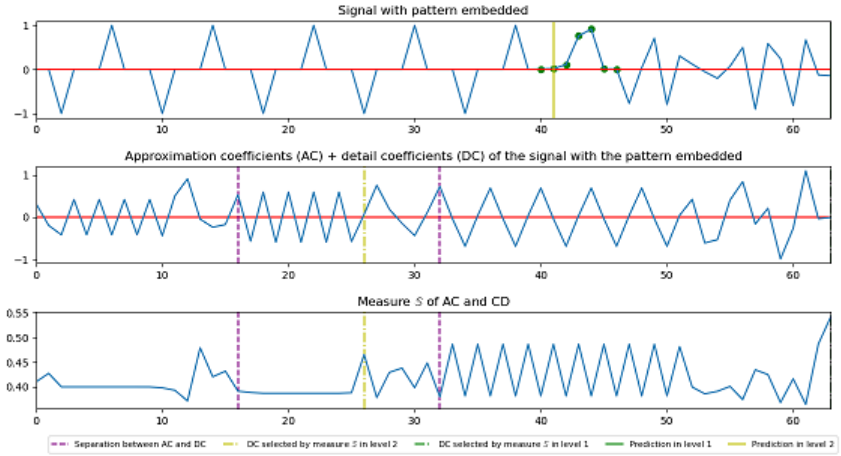

Figure 13: Detection of a dilated version of the pattern $m_2[\cdot]$.

Incorporating together the pattern $m_2[\cdot]$ and its dilated version into $f_2[\cdot]$ resulted in detecting the pattern at decomposition level 1, but not its subsampled version at level 2 (Figure 14).

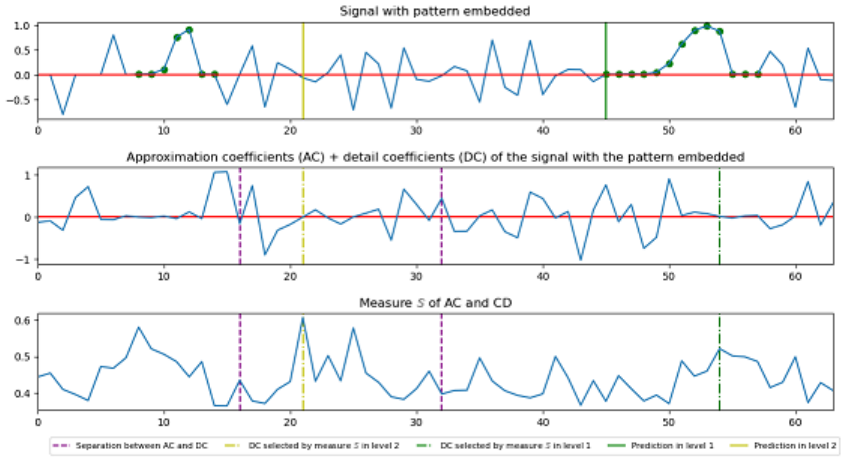

Figure 14: Joint detection of the pattern $m_2[\cdot]$ and its dilated version.

Respecting noise robustness, the detection of pattern $m_2[\cdot]$ for selected values of σ and λ is presented in Table 4, where a detection threshold of 5 samples was used. For both types of noise it is observed that by slightly perturbing the signal, the pattern is correctly detected, but by slightly increasing the noise level, the detection results become progressively worse, reflected in the decrease of the detection rate. Again, this is consistent with the results from [5, 6].

Gaussian noise			Poisson noise		
σ	Pattern detection counts	Detection rate	λ	Pattern detection counts	Detection rate
0.01	30	100%	0.01	24	80.00%
0.02	29	96.67%	0.02	16	53.33%
0.03	21	70.00%	0.03	19	63.33%
0.04	13	43.33%	0.04	13	43.33%
0.05	7	23.33%	0.05	8	26.67%

Table 4: Detection results for pattern $m_2[\cdot]$ after adding noise to the signal $f_2[\cdot]$. The pattern was detected with an error of up to 5 samples.

6. CONCLUSIONS

The case studies show that the approximation in the construction of the shapelet adapted to a given pattern depends on the numerical solution of the NLS to obtain the high-pass filters. In the experiments, the Powell's method with Anderson's initial guess was obtained as the best proposal. In this way filters with finite impulse response, compact support, and nearly linear phase response are obtained. The filter banks are, by construction, orthogonal and have perfect reconstruction property. To evaluate the performance of the shapelet to detect patterns, we propose to take the detail coefficient with measure $\mathbb{S}$ closer to one. The measure $\mathbb{S}$ value equal 1, used in [5, 6] is not reached.

As in reference works [5, 6], the results obtained show an improvement in detection with respect to other wavelet filters, which reaffirms its effectiveness.

The DST-II performs a successful detection of the pattern when it appears repeated within the input signal, however, the results are not the same when a subsampled version of the pattern appears. The detection of a dilated version of the pattern was successful, except when it is found between similar fragments of the signal. The wavelet bases created with the DST-II algorithm succeed in jointly detecting the presence of the original pattern and its dilation, verifying this theoretical assumption of the DST-II. It was confirmed that the detection algorithm is robust to changes in the amplitude of the patterns, with a lower precision in noisy signals.

The previous results lead us to, on the one hand, having to apply a noise attenuation process [2], if necessary, so that the detection of the required pattern is efficient, and on the other hand, to distinguish in some way the pattern location from other similar fragments in the signal.

This exploratory study brings several questions that have to be answer for using the DST-II in real problems: what is the impact of the iterative method of solving the system to construct the shapelet, as well as of the initial guess when using a large number of patterns?, will such methods work for patterns with larger numbers of samples?, could the behavior observed in this experiment be generalized to a larger variety of patterns?, will the numerical and detection parameters improve if pre–iteration is performed with any of the above mentioned methods, and will this improvement be statistically significant?, how effective would be the detection of a greater variety of signals with and without the presence of the patterns when compared to other wavelet filters?, will there be statistically significant differences between the parameters with respect to the numerical methods for solving the system? All these questions will be answered in further research.

ACKNOWLEDGMENTS

This research is part of the Project "Numerical methods for multiscale problems" associated to the National Program of Basic Sciences, Code PN223LH010-003, Ministry of Science, Technology and Environment (CITMA), Cuba, 2021-2023. The authors are grateful for the support of the Erasmus+ Program "Student Mobility for Traineeships" (2021) between the University of the Balearic Islands and the University of Havana.
This work has also been funded by the R+D+i project PID2019-104829RAI00 - "EXPLainable Artificial INtelligence systems for health and well-beING (EXPLAINING)", funded by MCIN/AEI/10.13039/501100011033, and is part of the R+D+i Project PID2020-113870GB-I00 - "Development of Soft Computing tools for Clinical Diagnostic Aid and Emergency Management (HESOCODICE)", funded by MCIN/AEI/10.13039/501100011033.

RECEIVED: AUGUST, 2022.
REVISED: FEBRUARY, 2023.

REFERENCES

[1] ANDERSON, D. G. (1965): Iterative Procedures for Nonlinear Integral Equations **Journal of the ACM**, 12(4):547–560.

[2] GOYAL, B., DOGRA, A., AGRAWAL, S., SOHI, B. S., AND SHARMA, A. (2020): Image denoising review: From classical to state-of-the-art approaches **Information Fusion**, 55(September 2019):220–244.

[3] GUIDO, R. C. (2011): A note on a practical relationship between filter coefficients and scaling and wavelet functions of discrete wavelet transforms **Applied Mathematics Letters**, 24(7):1257–1259.

[4] GUIDO, R. C. (2017): Effectively Interpreting Discrete Wavelet Transformed Signals **IEEE Signal Processing Magazine**, 34(3):89–100.

[5] GUIDO, R. C. (2018): Fusing time, frequency and shape-related information: Introduction to the Discrete Shapelet Transform's second generation (DST-II) **Information Fusion**, 41:9–15.

[6] GUIDO, R. C. (2021): Nearly symmetric orthogonal wavelets for time-frequency-shape joint analysis: Introducing the discrete shapelet transform's third generation (DST-III) for nonlinear signal analysis **Communications in Nonlinear Science and Numerical Simulation**, 97:1–12.

[7] GUIDO, R. C., BARBON, S., VIEIRA, L. S., SANCHEZ, F. L., MACIEL, C. D., PEREIRA, J. C., SCALASSARA, P. R., AND FONSECA, E. S. (2008): Introduction to the discrete shapelet transform and a new paradigm: Joint time-frequency-shape analysis In **Proceedings of the IEEE International Symposium on Circuits and Systems**, pages 2893–2896, Seattle, WA, USA.

[8] HADDADI, R., ABDELMOUNIM, E., HANINE, M. E., AND BELAGUID, A. (2014): Discrete Wavelet Transform Based Algorithm for Recognition of QRS Complexes **World of Computer Science and Information Technology Journal**, 4(9):127–132.

[9] LEE, G., GOMMERS, R., WASELEWSKI, F., WOHLFAHRT, K., AND O'LEARY, A. (2019): PyWavelets: A Python package for wavelet analysis **Journal of Open Source Software**, 4(36):1237.

[10] MALLAT, S. (2009): **A Wavelet Tour of Signal Processing: The Sparse Way** Academic Press, Burlington, 3rd edition.

[11] MESA, H. (2005): Adapted wavelets for pattern detection In Sanfeliu, A. and Cortés, M. L., editors, **Progress in Pattern Recognition, Image Analysis and Applications**, pages 933–944, Berlin, Heidelberg. Springer Berlin Heidelberg.

[12] MORÉ, J. J., GARBOW, B. S., AND HILLSTROM, K. E. (1980): User guide for MINPACK-1 Technical report, Argonne National Laboratory, Argonne, Illinois.

[13] OPPENHEIM, A. V. AND SCHAFER, R. W. (2011): **Tratamiento de señales en tiempo discreto** Pearson Educación, S.A., Ribera del Loira, Madrid, 3era edition.

[14] PANGANIBAN, A. (2012): Implementation of Wavelet Transform-Based Algorithm for Iris Recognition System **International Journal of Information and Electronics Engineering**, 2(3):328–332.

[15] PRESS, W. H., TEUKOLSKY, S. A., VETTERLING, W. T., AND FLANNERY, B. P. (2007): **Numerical Recipes: The Art of Scientific Computing** Cambridge University Press, 3rd edition.

[16] R. L. BURDEN, D. J. FAIRES, AND A. M. BURDEN (2017): Soluciones numéricas de sistemas de ecuaciones no lineales In **Análisis numérico**, pages 475–504. Cengage Learning, 10ma. edition.

[17] STRANG, G. AND NGUYEN, T. (1997): **Wavelets and filter banks** Wellesley-Cambridge, Wellesley, Massachusetts, revised 2nd edition.

[18] VIRTANEN, P., GOMMERS, R., AND OLIPHANT, P. . S. (2020): SciPy 1.0: Fundamental Algorithms for Scientific Computing in Python **Nature Methods**, 17:261–272.